rf cavity point-charge wakefield computation through a hybrid analytical and numerical approach

L. Shi[*]
Helmholtz-Zentrum Berlin, 12489 Berlin, Germany

Boris Podobedov[†]
Brookhaven National Laboratory, Upton, New York 11973, USA

(Received 8 July 2022; accepted 26 September 2022; published 13 October 2022)

We study short-range geometric wakefields of a normal conducting third harmonic cavity, developed by ALBA, which is currently under investigation for the BESSY II main storage ring upgrade. As is commonly done to enhance the shunt impedance, the single cell cavity shape includes smooth nose-cone transitions to the outside beam pipe, which significantly affects the wakefields. Utilizing the general approach developed by the earlier work [B. Podobedov and G. Stupakov, Phys. Rev. ST Accel. Beams **16**, 024401 (2013)], a model of point-charge wakefield for cavities of this type is suggested. The wakefield model consists of two parts: the singular part, inherently difficult for numerical codes, is found analytically, and the nonsingular part, which could be retrieved from relatively nondemanding numerical wakefield computations. Based on this hybrid approach, the wakefields due to arbitrary short bunches can be readily obtained both efficiently and accurately. The model was cross-checked against direct numerical simulations and a good agreement was found within the entire range of bunch lengths relevant to potential applications, from sub-millimeter down to 1-μm rms. We also observed that the wakefield model of a single cavity applies equally well to a small number of coupled cavities after some straightforward parameter scaling.

DOI: 10.1103/PhysRevAccelBeams.25.104602

I. INTRODUCTION

Collective effects often set performance limits for modern storage rings as well as for other types of accelerators. At high beam intensity, they typically cause significant deterioration of beam quality, instabilities, or other effects leading to rapid beam loss and in some cases could lead to damage of accelerator components. The most important collective effects are often those driven by the beam electromagnetic interaction with the vacuum chamber components, usually quantified in terms of wakefields in the time domain or (coupling) impedances in the frequency domain. Calculations of wakefields and impedances and the resulting collective effects they drive are therefore indispensable for the design of modern accelerators.

Analytical theories of wakefields and impedances due to various accelerator components have been developed over the last few decades [1,2]. They provide extremely valuable intuition and initial design guidance through the expressions for point-charge wakefield (Green's function wake) available for some very basic geometries and with some other simplifying assumptions. Nevertheless, due to the complexity of real-life accelerator components, as well as the high degree of confidence required for modern designs, the bulk of the wakefield calculations is presently done with 3D electromagnetic (EM) codes. These, in a nutshell, quantify the electromagnetic interaction of charged particles and the vacuum chamber from the first principles. Despite the explosive growth in available computing power, these calculations still require very substantial time and effort, and one is often forced to a compromise between accurately modeling a real-life structure (or a group of coupled structures) and what is realistic given the available time and resources.

The reason for this is threefold. First, for some accelerators, shorter and shorter bunches are becoming a reality, while some other machines, such as free-electron lasers, and, more recently, steady-state microbunching [3], intentionally introduce microstructures on top of the main bunch. Modeling single-bunch collective effects requires knowledge of the wakefields due to a much shorter bunch (or the microstructure) than the one envisioned for operations, e.g., due to the fact that single-bunch instabilities could potentially induce much shorter substructures on top

[*]liangliang.shi@helmholtz-berlin.de
[†]boris@bnl.gov

of the bunch. In practice, a factor of 10–15 between the operating rms bunch length σ and the driving bunch length, $\hat{\sigma}$, utilized in the EM code, is considered sufficient to obtain the wake (sometimes called pseudo-Green function) which could be used for subsequent beam dynamics calculations in place of an unknown point-charge wakefield [4,5].

Second, the short-range longitudinal wakefields are typically dominated by singularities, such that in the short bunch limit, they scale inversely to some power of the bunch length $W_{\parallel}^{\sigma}(s) \propto \sigma^{-q}$, $q > 0$ [2]. This implies that the wakefields for different bunch lengths are drastically different and that straightforward extrapolation of the wakefield effects toward shorter bunches does not work.

Finally, the required mesh size h used in EM codes must be a small fraction of $\hat{\sigma}$. Shorter bunches require progressively finer mesh size and correspondingly a larger number of mesh cells for a given structure volume. This translates to a larger required memory as well as longer CPU time needed to calculate the wakefield up to a fixed length $s_{\max}$. The CPU time scales as $1/h^3$ and $1/h^4$ for 2D and 3D structures, respectively [2].

Our present work was motivated by the need to evaluate the wakefields for a prototype design of a 1.5 GHz, active, third harmonic rf cavity planned to replace the existing aging passive Landau cavities at BESSY II [6,7]. The new cavity was originally developed by ALBA and is now undergoing further development and testing under a collaboration among CELLS, HZB, and DESY [8]. This new cavity design will allow for stretching the bunch by a factor of 2–3 compared to the presently available 20% lengthening; the beam lifetime will lengthen proportionally. It will also provide an option of significantly shortening the bunch at low currents, where the final bunch length is expected to be well into the sub-millimeter region. In the future, the same or similar cavity design is envisioned for MLS, BESSY III, and MLS II [9,10], and, in all cases, the short-bunch collective beam dynamics is expected to be of great importance. This motivated us to seek a point-charge wakefield model, so we could predict the wakefields due to arbitrary short bunches.

For a fairly common case when multiple rf cavities are installed next to each other, their short-range wakefields interfere. Therefore, we have also studied this possibility.

Even for a single cavity, a brute force numerical calculation of short-bunch wakefields could be extremely demanding. For the bunch length of a few millimeters, it requires billions of mesh cells in 3D geometry computations, and for sub-mm bunches, they are not possible with our available computing resources (Intel Xeon E5 with 12 core and 256 GB RAM). This is why, in this paper, we follow the general approach from [11,12], which outlined how to accurately find point-charge geometric wakefields for arbitrary accelerator structures, utilizing some general analytical results as well as numerical computations with EM codes for relatively long bunches. Specifically, the short-range wakefield is separated into two parts: the singular part, inherently difficult for numerical codes, is found analytically, and the nonsingular part, which is retrieved from relatively non-demanding numerical wakefield computations by using low-order polynomial fitting. Finally, at a longer range (which is not the focus of this paper), where the wakefields weakly depend on the bunch length, one could well approximate the point-charge wakefields with those found numerically, again with a relatively long drive bunch.

With the point-charge wakefield model in hand, one could easily find the wake potential due to an arbitrary long bunch by convolution with the charge density (assumed Gaussian throughout this paper). To show that our point-charge wakefield models in the longitudinal and transverse planes are indeed accurate, we extensively cross-checked the wakefields found from these models by convolution to those calculated directly with EM codes.

In this paper, we stay within the usual ultrarelativistic approximation, $\gamma \gg 1$. Throughout the paper, we use SI units. For wakefields and related quantities, we follow the definitions from [2]. In particular, our sign convention is that $s < 0$ is ahead of the bunch, a negative longitudinal wakefield corresponds to the energy loss, and a positive transverse wakefield is defocusing.

The rest of this paper is organized as follows: We first present the analytical model of wakefield for our nose-cone cavity in Sec. II. The model is validated and compared with direct simulations in Sec. III, where the wakefield singular behavior, parameter scaling, and the equivalent geometries are also discussed. We conclude the paper in Sec. IV.

II. ANALYTICAL WAKEFIELD MODEL FOR A NOSE-CONE CAVITY

The rf cavity under consideration is of the nose-cone type (sometimes also called reentrant). It resembles a pillbox cavity but with smooth nose cones to enhance the shunt impedance of the fundamental mode with respect to higher order modes. Our particular cavity geometry, shown in Fig. 1, is a variant of [7] and it has an axial symmetry for the cavity body under prototyping. The cavity also possesses longitudinal midplane symmetry. The cavity is 87 mm long and has two beam pipes of 23 mm in radius on each side. The radial profile of the nose cones is an arc of a circle with 4 mm in radius, as marked in the vicinity of points P0, Q0, P1, and Q1 in Fig. 1.

The bunch length σ within our application interests ranges from 1 μm to sub-millimeter. In the following, we will develop the point-charge wake function model, which, in principle, allows one to reconstruct the wake potential due to an arbitrary short bunch length.

The short-range wakefield is formed in the following process: when a point charge, traveling with the speed of light, traverses this cavity, its pancake field scatters at the discontinuity points of the radial boundary derivative, located along cross-sections P0-Q0 and P1-Q1. The scattered spherical wave fronts eventually catch up with the

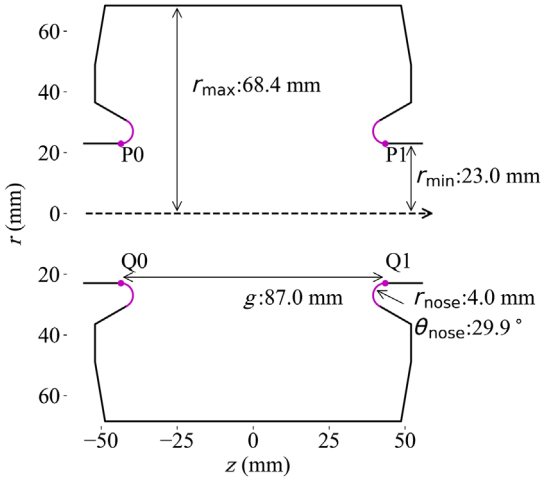

FIG. 1. rf cavity geometry with key points and dimensions labeled.

charge and therefore define the wake function at $s = 0$. By causality, all other scattered fields must follow with some delay, thus contributing to the wake function at some distance $s > 0$ behind the charge.

As was pointed out in [11], there always exists a length parameter $\lambda_g > 0$, which defines the s location of the singularity in the wake function or its derivatives that are closest to (but not at) the origin. The wake potential calculated for a short enough bunch, $\hat{\sigma} \ll \lambda_g$, contains enough information to reconstruct the wake for arbitrarily short bunch, including the point-charge wake.

The parameter λ_g can be easily found by analyzing the critical points of the boundary and selecting the path which results in the minimum nonzero delay. Reference [11] provides instructive examples of calculating λ_g for typical cavitylike or collimatorlike geometries. For any cavity of the shape similar to that in Fig. 1, this parameter is given by

$$\lambda_g = \min\left(\sqrt{4r_{\rm min}^2 + {\rm g}^2} - {\rm g}, \sqrt{4\{\Delta r - r_{\rm nose}[1-\cos(\phi)]\}^2 + [{\rm g} - 2r_{\rm nose}\sin(\phi)]^2} + 2r_{\rm nose}\phi - {\rm g}, 2{\rm g}\right) \tag{1}$$

where $\Delta r = r_{\rm max} - r_{\rm min}$ and the angle $\phi < \pi/2$ is

$$\phi = 2\arctan\left(\frac{-\frac{\rm g}{2} + \sqrt{\Delta r^2 - 2\Delta r\, r_{\rm nose} + \frac{{\rm g}^2}{4}}}{\Delta r - 2r_{\rm nose}}\right). \tag{2}$$

Here, the first element in the set, $\sqrt{4r_{\rm min}^2 + {\rm g}^2} - {\rm g}$, corresponds to the delay acquired for the scattered field traveling from point P0 to Q1, or, equivalently, from Q0 to P1. The second element is due to the field path from P0 to the nearest point in the cavity midsection, $z = 0$, $r = r_{\rm max}$, and then to P1 (or an equivalent path starting at Q0), with ϕ being the angle of the path along the nose-cone surface. This path would typically be the shortest for shallow cavities. The last element of the set in Eq. (1), defining λ_g for short cavities, is due to the reflections at the beginning and the end of the cavity.

For the particular cavity dimensions shown in Fig. 1, the first element in the set in Eq. (1) is the smallest, so

$$\lambda_g = \sqrt{4r_{\rm min}^2 + {\rm g}^2} - {\rm g} = 11.4\ {\rm mm}. \tag{3}$$

Note that this equation is the same as for the λ_g parameter for the straight cylindrical cavity with equivalent dimensions, i.e., the nonlinear tapering due to the nose cones does not affect this parameter. This is in contrast to the cavity with a gradual linear taper [the case treated in Ref. [11], see Eq. (17)], where the λ_g parameter is proportional to the square of the tapering angle and would typically be much smaller for similar cavity dimensions.

The longitudinal wake potential of the cavity shown in Fig. 1, calculated with the code ECHO [13] for $\sigma = 0.5$ mm bunch, is shown in Fig. 2 with λ_g indicated by the vertical dashed line. The figure also includes the derivative of the wake potential plotted on the right axis. As will be shown later, the singular behavior of the wakefield at $s = 0$ can be described by the diffraction model (see, e.g., [1,2,14,15]) together with another singularity [16] coming from the nonlinear transitions at the nose cones.

The location of the next "special" point in the wake plotted in Fig. 2, at $s = \lambda_g = 11.4$ mm, is clearly identifiable from the dip in the wake potential derivative. Here

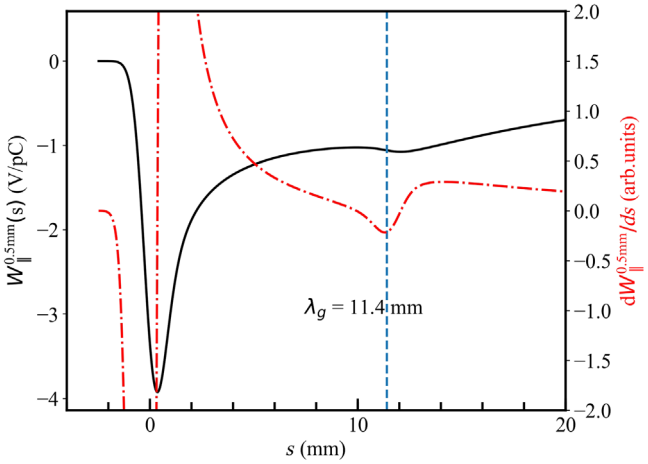

FIG. 2. The rf cavity wake potential (solid black line), its derivative (dash-dotted red line, right axis), and the s position which corresponds to the λ_g parameter (dashed blue line).

the point-charge wake derivative is discontinuous, and therefore the second derivative of the wake potential is singular (divergent for $\sigma \to 0$). However, apart from identifying the location of this point from Eq. (3), we will not be relying on any knowledge of the wake behavior in the vicinity.

Instead, we will concentrate on obtaining the short-range wake potentials spanning up to 5σ in most cases, for σ values from 1 μm to sub-millimeter. Following [11,12], to calculate these, we will rely on numerical calculations with the driving bunch length $\hat{\sigma}$ much shorter than λ_g, even though $\hat{\sigma} \gg \sigma$ will hold in most cases. These calculations will also be used to construct the short-range point-charge wake model. For our geometry and the corresponding parameter $\lambda_g = 11.4$ mm, we chose $\hat{\sigma} = 0.5$ mm $\ll \lambda_g$.

A. Longitudinal wakefield

Following [11], the analytical wake function is proposed to be the sum of a nondivergent part, usually well represented by a linear polynomial, $\alpha + \beta s$, and a singular part. For the nose-cone cavity, we find that the singular part contains not only the usual diffraction model $\propto s^{-1/2}$ but also a term $\propto s^{-1/3}$. The longitudinal wake function thus takes the form:

$$W_{\parallel}^{\delta}(s) = \alpha + \beta s + k_d s^{-1/2} + k_s s^{-1/3} (0 < s < \lambda_g), \tag{4}$$

where the parameters α, β, k_d, and k_s depend on the cavity geometry. The coefficient k_d is given by the diffraction model (see, e.g., [1,2,14,15]),

$$k_d = -\frac{Z_0 c}{\pi^2} \frac{\sqrt{g/2}}{r_{\min}}, \tag{5}$$

The last term in Eq. (4) is due to the smooth transitions from the nose cones to the straight pipe. We find that it is critical to include this singular contribution in the cavity model for an accurate short-range wake potential reconstruction; otherwise, it overestimates the magnitude of the wake. The $s^{-1/3}$ singularity due to such type of transition was first derived in Ref. [16] for a taper-in geometry. For a slowly varying transition of parabolic shape with the first derivative of the radial boundary matched to zero at $r_{\min}$, the $s^{-1/3}$ singular part of the point-charge wake has the coefficient

$$k_s^{\text{tap}} = \frac{Z_0 c}{2\pi r_{\min}} (6r'')^{-1/3}, \tag{6}$$

where r'' stands for the second derivative of the parabolic radial boundary with respect to the axial coordinate.

Close to the minimum radius, the nose cones are essentially parabolic, with $r'' = 1/r_{\text{nose}}$, so one would expect the expressions for k_s and k_s^{tap} to be identical except for a numerical coefficient on the order of 1. However, because we lack the exact coefficient for the nose-cone cavity geometry, in this paper, we obtained the parameter k_s in Eq. (4) by fitting the wake potentials as explained in the next section. Note that, unlike k_d, the coefficient k_s is positive, i.e., the $s^{-1/3}$ singular term due to smooth nose cones counteracts the dominant term due to the diffraction model, reducing the total wake by absolute value.

The wake potential for a bunch distribution $\lambda(z)$ is given by the convolution of $\lambda(z)$ and the wake function given in Eq. (4). For a Gaussian bunch, $\lambda(z) = \frac{1}{\sqrt{2\pi}\sigma} e^{-\frac{z^2}{2\sigma^2}}$, this convolution can be efficiently evaluated numerically and can also be written in the closed form [11]:

$$W_{\parallel}^{\sigma}(s) = \left(\frac{\alpha}{2} + \sigma\frac{\beta u}{2}\right)\left[1 + \text{erf}\left(\frac{u}{\sqrt{2}}\right)\right] + \frac{\beta\sigma}{\sqrt{2\pi}} e^{-u^2/2} + k_d \sigma^{-1/2} f_1(u) + k_s \sigma^{-1/3} f_2(u), \tag{7}$$

where $u = s/\sigma$ is a normalized distance, $\text{erf}(\cdot)$ is the error function, $f_1(\cdot)$ and $f_2(\cdot)$ are two auxiliary functions given by

$$f_1(u) = \text{e}^{-\frac{u^2}{4}} \sqrt{\frac{\pi}{8}|u|}\left[I_{-1/4}\left(\frac{u^2}{4}\right) + \text{sign}(u) I_{1/4}\left(\frac{u^2}{4}\right)\right]$$

$$f_2(u) = p\left[u_1 F_1\left(\frac{2}{3};\frac{3}{2};-\frac{1}{2}u^2\right) + q_1 F_1\left(\frac{1}{6};\frac{1}{2};-\frac{1}{2}u^2\right)\right],$$

where $p = \pi^{-\frac{1}{2}} 2^{-\frac{2}{3}} \Gamma(\frac{5}{6})$, $q = \pi^{-1} 2^{-\frac{3}{2}} \Gamma(\frac{1}{6})\Gamma(\frac{1}{3})$, and $\Gamma(\cdot)$, the gamma function, $I_v(\cdot)$, the modified Bessel function of the first kind with order and ${}_1F_1(\cdot)$, the confluent hypergeometric function of the first order.

We can now establish how the wakes, as well as the individual coefficients in Eqs. (4) and (7), scale with the cavity dimensions. If we uniformly scale all cavity dimensions as well as the bunch length by a factor η, then the resulting wake potential will be related to the original one by

$$W_{\parallel,\eta}^{\sigma\cdot\eta}(s\cdot\eta) = \frac{1}{\eta} W_{\parallel,\eta=1}^{\sigma}(s). \tag{8}$$

This scaling is exact for an arbitrary structure and bunch length. The equivalent expression (with both superscripts replaced by δ) also holds for the point-charge wakes. Therefore, the coefficients α, β, k_d, k_s of the scaled structure relate to the original ones by factors of $1/\eta, 1/\eta^2, \eta^{-1/2}, \eta^{-2/3}$, respectively. These relations could be useful when cross-checking numerical codes.

Alternatively, if only the longitudinal cavity dimensions are scaled by a factor κ, while the transverse dimensions are left intact, and the bunch length is scaled by $1/\kappa$, it immediately follows from Eqs. (5)–(7) that, for short bunches,

$$W^{\sigma/\kappa}_{\parallel,\kappa}(s/\kappa) \approx \kappa W^{\sigma}_{\parallel,\kappa=1}(s). \tag{9}$$

Here the equality is only approximate because we neglected the nonsingular parts, which become progressively small as the bunch gets shorter. This scaling law is very useful for the numerical wake computations. If the bunch is stretched by a factor of $1/\kappa > 1$ while the structure is compressed longitudinally by a factor of $\kappa < 1$, this leads to a drastic reduction of the number of required mesh cells and thus the computational power. We will take advantage of this relation in Sec. III when dealing with the direct computation of wake potentials due to the shortest drive bunch of $\hat{\sigma} = 1$ μm.

It should be noted that Eq. (9) was derived previously (under several assumptions with regard to the boundary variation) for a wide range of accelerator structures by means of parabolic equation approach to Maxwell's equations [17]. The same reference also pointed out the utility of Eq. (9) for the numerical calculation of wake potentials.

B. Transverse wakefield

The general form of the transverse wakefield could be obtained by integrating the longitudinal one (and omitting the constant term because $W^{\delta}_{\perp}(0) = 0$ [2]). Keeping all signs positive, and introducing the first three terms consistent with [12], it is proposed as

$$W^{\delta}_{\perp}(s) = \alpha_{\perp} s + \beta_{\perp} s^2 + 2k_{d,\perp} s^{1/2} + \frac{3}{2} k_{s,\perp} s^{2/3} (s > 0), \tag{10}$$

where the parameters $\alpha_{\perp}$, $\beta_{\perp}$, $k_{d,\perp}$, and $k_{s,\perp}$ depend on the cavity geometry. In contrast to the longitudinal case, the transverse wake function shows no singular behavior at $s = 0$.

As usual, by the transverse wakefield for the axially symmetric geometry, we mean the dominant $m = 1$ dipole mode. Therefore, we generally cannot rely on the Panofsky-Wenzel theorem [18] to relate the coefficients in the transverse wake in Eq. (10) and the $m = 0$ longitudinal wake in Eq. (4). To emphasize that the coefficients in this section are different, they carry an added "$\perp$" subscript. These coefficients need to be found separately from the corresponding longitudinal ones.

The diffraction model term in Eq. (10) is, of course, well known, and its coefficient is given by (see, e.g., Refs. [1,2,14,15])

$$k_{d,\perp} = \frac{Z_0 c}{\pi^2} \frac{\sqrt{2g}}{r^3_{\min}}. \tag{11}$$

The rest of the coefficients in Eq. (10) can be found by fitting the wake potentials. Similar to the longitudinal case, we find that $k_{d,\perp}$ and $k_{s,\perp}$ are of opposing signs (i.e., $k_{s,\perp} < 0$), so the last term in Eq. (10) counteracts the diffraction model term, somewhat reducing the magnitude of the total wake.

Performing a convolution of Eq. (10) with a Gaussian bunch distribution, we get the transverse wake potential

$$\begin{aligned} W^{\sigma}_{\perp}(s) = {} & \frac{\alpha_{\perp} s + \beta_{\perp}(s^2 + \sigma^2)}{2} \left[1 + \operatorname{erf}\left(\frac{1}{\sqrt{2}} u\right)\right] \\ & + \frac{(\alpha_{\perp} + s\beta_{\perp})\sigma}{\sqrt{2\pi}} e^{-u^2/2} + k_{d,\perp} \sigma^{\frac{1}{2}} \int_{-\infty}^{u} f_1(u) du \\ & + k_{s,\perp} \sigma^{\frac{2}{3}} \int_{-\infty}^{u} f_2(u) du, \end{aligned} \tag{12}$$

where $u = s/\sigma$, $f_1(\cdot)$, and $f_2(\cdot)$ are the same as in the longitudinal definition given after Eq. (7). The integrals above can be expressed as

$$\begin{aligned} \int_{-\infty}^{u} f_1(u) du = {} & e^{\frac{-u^2}{4}} \sqrt{\frac{\pi}{8|u|}} \left\{ (u^2 + 2) I_{1/4}\left(\frac{u^2}{4}\right) + u^2 I_{5/4}\left(\frac{u^2}{4}\right) \right. \\ & \left. + u^2 \operatorname{sign}(u) \left[I_{-1/4}\left(\frac{u^2}{4}\right) + I_{3/4}\left(\frac{u^2}{4}\right) \right] \right\}, \\ \int_{-\infty}^{u} f_2(u) du = {} & \frac{1}{4\sqrt{\pi}} \left[2^{5/6} \Gamma\left(\frac{1}{3}\right) u_1 F_1\left(\frac{1}{6}; \frac{3}{2}; -\frac{1}{2} u^2\right) \right. \\ & \left. + 3 \times 2^{1/3} \Gamma\left(\frac{5}{6}\right) {}_1F_1\left(-\frac{1}{3}; \frac{1}{2}; -\frac{1}{2} u^2\right) \right]. \end{aligned}$$

According to Eq. (12), as the bunch gets shorter, the transverse wake potential goes to zero as expected.

Similar to the longitudinal case, we can now establish some useful scaling laws for the transverse wakes. The transverse equivalent of Eq. (8), i.e., the exact relation of the wake potentials before and after the scaling of all cavity dimensions and the bunch length by the same factor η is given by

$$W^{\sigma\cdot\eta}_{\perp,\eta}(s \cdot \eta) = \frac{1}{\eta^2} W^{\sigma}_{\perp,\eta=1}(s). \tag{13}$$

Therefore the transverse coefficients, $\alpha_{\perp}$, $\beta_{\perp}$, $k_{d,\perp}$, and $k_{s,\perp}$, scale as $1/\eta^3, 1/\eta^4, \eta^{-5/2}, \eta^{-8/3}$.

For longitudinal-only dimension scaling, the analog to Eq. (9) in the transverse plane is given by

$$W^{\sigma/\kappa}_{\perp,\kappa}(s/\kappa) \approx W^{\sigma}_{\perp,\kappa=1}(s), \tag{14}$$

which again conforms to an earlier finding in Ref. [17]. Similar to its longitudinal equivalent, this scaling relation provides significant computational benefits and will be exploited later for the numerical calculations of wake potentials due to the shortest drive bunch of $\hat{\sigma} = 1$ μm.

III. NUMERICAL SIMULATION AND COMPARISON WITH WAKE MODEL

A number of numerical codes have been developed for geometric wakefield computations, including ABCI [19], ECHO [13], ACE3P [20], CST [21], GdfidL [22], and some others. Most of them can handle realistic 3D geometries. However, for our cavity, the components like various dampers, the input power port, etc. that break the axial symmetry do not contribute to the short-range wakefield formation and therefore do not affect the short-range wake potentials. The validity of this assumption has been cross-checked with a 3D simulation of the full cavity for a bunch of 2 mm rms length. On the other hand, by exploiting the axial symmetry, we can reduce the required computing power by orders of magnitude. Therefore, we stay with the axially symmetric cavity geometry as shown in Fig. 1 and utilize ECHOz1 and ECHOz2 [13]—the versions of ECHO that, respectively, can efficiently calculate the longitudinal and transverse wake potentials of axially symmetric structures.

As the bunch length decreases to the level of about 10 μm, even the 2D model computations with ECHO take up prohibitive memory and computing time. To proceed there, we take advantage of the allowed volume-reducing modifications to the cavity geometry which preserve the point-charge wake up to some maximum distance, as was discussed in [11]. For instance, three different cavities with the radial profiles shown in Fig. 3 must have exactly the same point-charge wakefield up to some distance $s_{\max}$, which is equal to the smallest λ_g parameter of the three profiles. Therefore, the corresponding wake potentials due to a bunch of finite length σ will also be equal up to the same distance $s_{\max}$ minus a few σ.

To illustrate this further, in Fig. 4, we show the wake potentials due to 25-μm bunch calculated for the cavities with profiles 1 and 2 shown in Fig. 3. As expected, the two cavities share the same wake potential until the discrepancy occurs near $s_{\max} = \lambda_g|_{\text{profile 1}} = 368$ μm, where the parameter λ_g for profile 1 is defined by the second term in Eq. (1). Similarly, the short-bunch wake potential of the cavity with profile 3 will deviate from the original one (profile 2) only at s positions greater than 11.4 mm, which is the λ_g value for the original cavity (see Fig. 2).

Since the cavity with profile 1 has much less area to mesh compared with the original cavity, and it results in the same short-range wake, it has been used for the calculation of the wake potentials due to $\hat{\sigma} = 10$ μm bunch up to the wake length up to $5\hat{\sigma}$ to be presented below.

A. Single cavity

As was mentioned earlier, ECHO-calculated wake potentials for a bunch with $\hat{\sigma} = 0.5$ mm are used to construct the point-charge wake function models in the longitudinal and transverse planes. Specifically, the diffraction model wake potential is subtracted from the

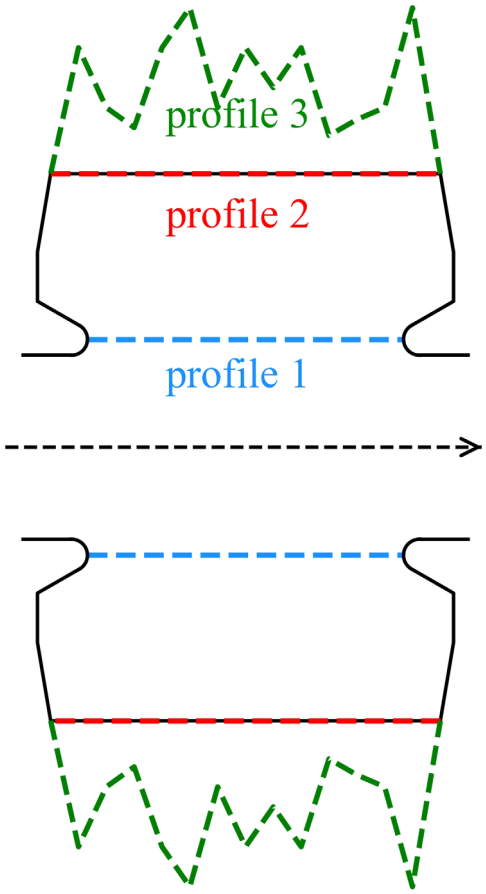

FIG. 3. Three equivalent geometries with different outer wall boundaries, which result in the same short-range wake up to some distance $s_{\max}$. Profile 1 corresponds to a shallow cavity with the radius $r_{\max} = 27$ mm. Profiles 2 corresponds to the original cavity of Fig. 1 with $r_{\max} = 68.4$ mm. Profile 3 represents a cavity with an arbitrary outer wall variation, and $r_{\max}(s) > 68.4$ mm.

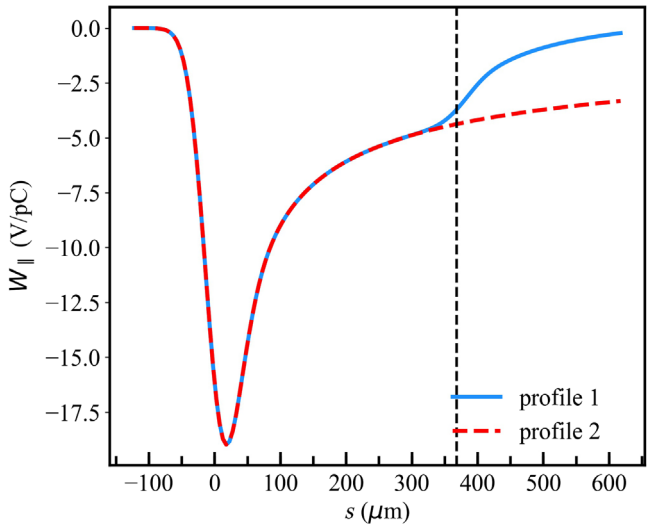

FIG. 4. Wake potentials due to a bunch with $\sigma = 25$ μm for the cavities with profile 1 (solid blue) and 2 (dashed red). The black dashed line indicates the value of λ_g parameter for the cavity with profile 1.

numerically calculated total wake potential. The residual, taken in the s range of $[-3\hat{\sigma}, 3\hat{\sigma}]$, is then used to fit the model, Eqs. (7) and (12), and obtain the parameters $\alpha(3.68\times10^{-2})$, $\beta(-6.95\times10^{1})$, $k_s(7.30\times10^{-2})$ for the longitudinal wake and $\alpha_\perp(-4.56\times10^{2})$, $\beta_\perp(-1.78\times10^{4})$, $k_{s,\perp}(-1.83\times10^{2})$ for the transverse wake. Note that including the term $s^{-1/3}$ in Eq. (4) was important. Performing the fit (and the reconstruction) without the term would, for instance, at $\sigma = 100$ μm, produce the reconstructed wake potential about 15% higher in amplitude than the actual one. Once we obtain these parameters, the wake potentials for an arbitrary short bunch are readily available from Eqs. (7) and (12).

The comparisons between the directly simulated wake potentials and the reconstructed ones based on our wake models are shown in Figs. 5 and 6 for the longitudinal and transverse directions, respectively. Direct calculations of the wake potentials due to a 100 μm drive bunch was performed for the original cavity shape. To speed up the computations, the wake potential due to a drive bunch of 10 μm was calculated for the cavity with profile 1 in Fig. 3. In the 1 − μm case, we additionally relied on the scaling laws from Eqs. (9) and (14). Specifically, we used the scaling factor $\kappa = 1/5$ so that the cavity with profile 1 was compressed longitudinally by a factor of 5 while the drive bunch was stretched to $\hat{\sigma} = 5$ μm.

As evidenced by Figs. 5 and 6, the wake potentials from our point-charge wake function models agree perfectly well with the direct simulation results in both longitudinal and transverse cases.

As a reminder, while studying the wake potentials due to very short bunches, we assumed the infinite beam energy ($\gamma \to \infty$) throughout the paper. This assumption allows for the impedance to extend to an infinite frequency, corresponding to the wake singularity at $s = 0$.

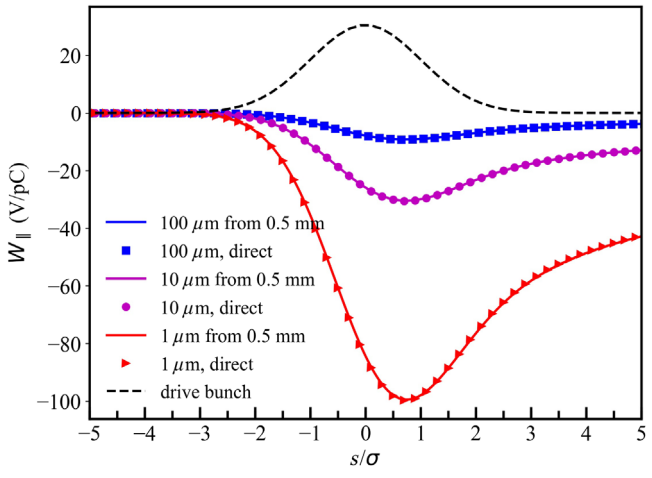

FIG. 5. Comparison of the reconstructed longitudinal wake potentials (solid lines) with direct ECHO simulations (symbols) performed at several rms bunch lengths, as indicated in the legend.

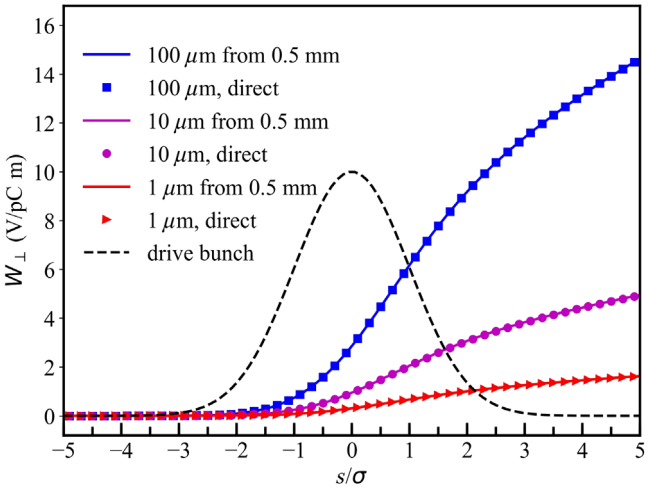

FIG. 6. Comparison of the reconstructed transverse wake potentials (solid lines) with direct ECHO simulations (symbols) performed at several rms bunch lengths, as indicated in the legend.

However, at finite beam energies, the geometric impedance high-frequency cutoff occurs at $\omega \approx \gamma c/r_{\min}$, which, equivalently, limits the wake potentials for bunches shorter than $r_{\min}/\gamma$ [1].

B. Coupled cavities

We have two main motivations to study a structure with multiple coupled cavities. First, it is intriguing to find out if the $s^{-1/3}$ singular form of the single cavity, still holds in this case. Second, from a practical perspective, at least three harmonic cavities will be needed in order to achieve the optimal bunch lengthening for the BESSY II upgrade. We thus consider the case where up to four cavities, as an upper limit, are installed next to each other, which is the current configuration for BESSY II. As will be shown later, accounting for the cavities individually will overestimate the wake potentials due to the interference of the short-range wakefields, which are coupled via the connecting beam pipe due to $\sigma \ll r_{\min}$.

A sketch of this structure where four cavities are coupled via the beam pipe is shown in Fig. 7. The overall length of the structure we consider is about 1 m.

To study the wakefields of this structure, we parameterize them in exactly the same way as we did for the single cavity in Eqs. (4) and (10) and then find the respective coefficient by

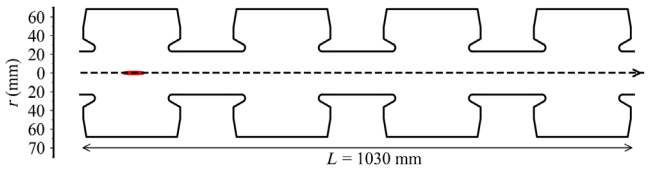

FIG. 7. Four-cavity structure. Each cavity is identical to the one in Fig. 1 and the center-to-center spacing is 314.3 mm.

fitting a numerically calculated wake potential. In contrast to the single cavity case, where the analytical expression for k_d ($k_{d,\perp}$) was readily available, here we also fit this parameter. For this structure, the parameter λ_g is determined similarly as for the single cavity, Eqs. (1)–(3), except the relevant critical points, which are located at the nose cones at the entrance and exit of the entire structure. Therefore, they are separated by $g = 1030$ mm. The corresponding parameter λ_g is now smaller and according to Eq. (3), the new value is approximately 1 mm. We thus used a bunch with $\hat{\sigma} = 0.2$ mm $\ll \lambda_g$ to construct the wake function models for the coupled cavity structure.

The fitted parameters amount to 2.61×10^{-1}, -2.31×10^{3}, -3.24×10^{-1}, 3.48×10^{-2} for α, β, k_d, k_s in the longitudinal model and for the transverse model 2.49×10^{4}, -4.92×10^{6}, 1.45×10^{3}, -1.54×10^{3} for $\alpha_\perp, \beta_\perp, k_{d,\perp}, k_{s,\perp}$, respectively. The resulting longitudinal and transverse wake potentials are shown in Figs. 8 and 9, respectively. The solid lines show the reconstructed wake potential, while the symbols represent the wake potentials calculated directly for the four-cavity structure. Similar to the single cavity case, we observe a perfect agreement between the directly calculated wake potentials and the ones found in our model. This argues that our approach to finding the short-range wakes works equally well for the case of coupled cavities and that the models given by Eqs. (4) and (10) do not require any extra terms in this case.

Also shown in Figs. 8 and 9 are the dash-dotted curves representing four times the respective wake potentials due to a single cavity. Clearly, a simple quadrupling of the wake potential due to a single cavity overestimates the wake potential of the four-cavity structure.

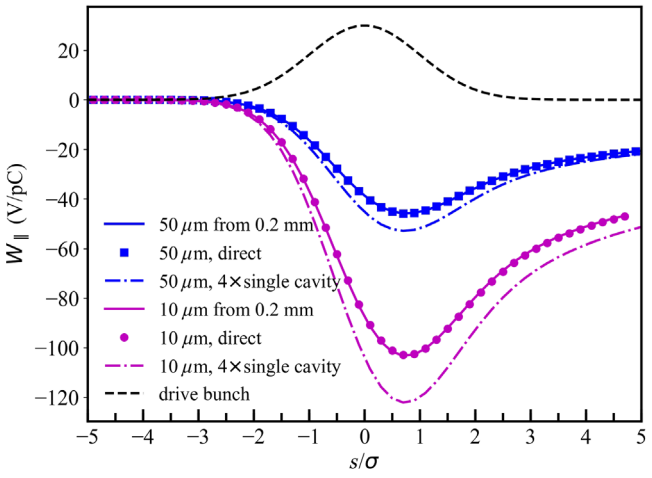

FIG. 8. Comparison of the reconstructed longitudinal wake potential (solid lines) due to various σ (indicated in legend) with direct simulation for the four-cavity structure (symbols). The dash-dotted lines show four times the wake potential for a single cavity at the indicated bunch length.

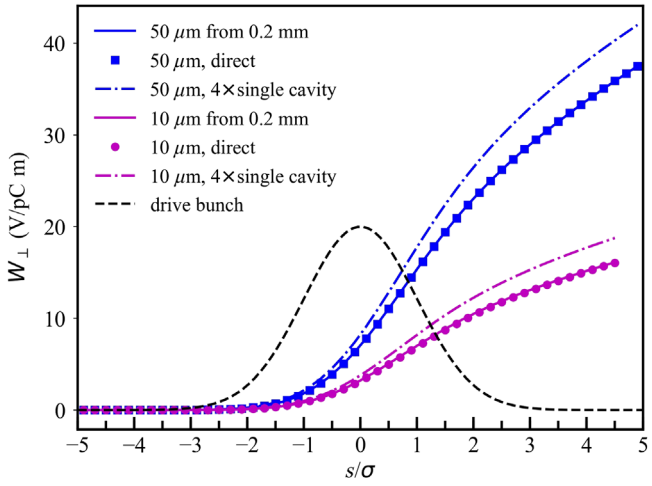

FIG. 9. Comparison of the reconstructed transverse wake potential (solid lines) due to various σ (indicated in legend) with direct simulation for the four-cavity structure (symbols). The dash-dotted lines show four times the wake potential for a single cavity at the indicated bunch length.

To illustrate this effect over a wide range of bunch lengths, we have also looked at the loss factor $\kappa_\parallel$ and the kick factor $\kappa_\perp$. These quantities, frequently used in studies of collective beam dynamics, are defined as

$$\kappa^{\sigma}_{\parallel,\perp} = \int_{-\infty}^{\infty} W^{\sigma}_{\parallel,\perp}(s)\lambda(s)ds. \tag{15}$$

For our wake models, they can be explicitly expressed as

$$\kappa^{\sigma}_{\parallel} = \frac{\alpha}{2} + \frac{\beta}{\sqrt{\pi}}\sigma + \frac{1}{2\sqrt{2\pi}}\Gamma\left(\frac{1}{4}\right)k_d\sigma^{-1/2} + \frac{1}{2^{4/3}\sqrt{\pi}}\Gamma\left(\frac{1}{3}\right)k_s\sigma^{-1/3}, \tag{16}$$

$$\kappa^{\sigma}_{\perp} = \frac{\alpha_\perp}{\sqrt{\pi}}\sigma + \beta_\perp\sigma^2 + \sqrt{\frac{2}{\pi}}\Gamma\left(\frac{3}{4}\right)k_{d,\perp}\sigma^{1/2} + \frac{3}{2^{4/3}\sqrt{\pi}}\Gamma\left(\frac{5}{6}\right)k_{s,\perp}\sigma^{2/3}. \tag{17}$$

These factors, calculated for the single cavity and the four-cavity structure, are shown in Fig. 10.

Clearly, the single cavity model overestimates the loss and kick factors per cavity compared to the four-cavity model. The absolute discrepancy is more pronounced for shorter bunches in the longitudinal case and for longer bunches in the transverse case. The relative deviation, over the range of σ shown, decreases with σ from about 25% to 15% for the longitudinal case while staying roughly constant, at around 15%, for the transverse case. Note that for very short bunches, the loss (kick) factor is

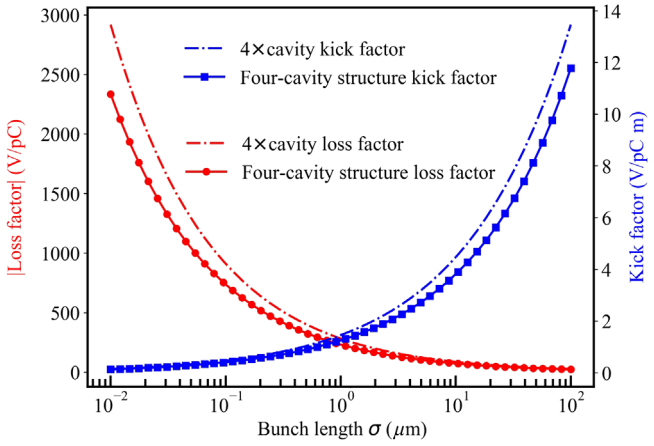

FIG. 10. The absolute value of the loss factor and the kick factor for the four-cavity structure (solid lines with symbols). Four times the equivalent quantities for a single cavity are shown in the dash-dotted lines.

dominated by the diffraction model and scales roughly as $\propto\sigma^{-0.5}(\propto\sigma^{0.5})$, see Ref. [15].

At a given bunch length, the loss and kick factors are entirely defined by three geometric parameters: the minimum radius r_{min}, the cavity length g, and the nose radius r_{nose}. Once these parameters are fixed, there is no chance to optimize the loss and kick factors for short bunches.

IV. CONCLUSION

We presented a way to accurately calculate the short-range wakefield of the third harmonic rf cavity, which is currently being considered for BESSY II. Our method produces a model of the point-charge wakefield and is, therefore, capable to construct the wake potential due to an arbitrarily short bunch. The point-charge wakefield model has two singular terms that diverge at the origin as $s^{-1/2}$ and $s^{-1/3}$, which result in the divergent terms $\sigma^{-1/2}$ and $\sigma^{-1/3}$ in the wake potential. We showed that in spite of smooth nose-cone transitions at the minimum cross section, the parameter λ_g for this cavity is the same as for a straight cylindrical cavity of the same length. This is in contrast to the cavity with a gradual linear taper (treated in Ref. [11]), where the corresponding parameter is proportional to the square of the tapering angle and would typically be much smaller for similar cavity dimensions. A large λ_g parameter for the nose-cone cavity allowed us to accurately find the point-charge wakefield by fitting the numerically obtained wake potential due to a relatively long bunch, $\hat{\sigma} = 0.5$ mm. This wakefield model was cross-checked against direct simulations at various bunch lengths in the 1–100 μm range and they were shown to agree well with each other.

Separately, we studied the case of a small number of cavities of this type, which are coupled together. We established that the wakefield model of a single cavity, given by Eqs. (4) and (10), applies equally well to this case after some straightforward scaling of the numerical coefficients. In agreement with the expectation from earlier works [1], the total wakefield of this multicavity system ended up smaller than the sum of the individual cavity wakefields, with this effect becoming more pronounced for shorter bunches.

While we analyzed a particular cavity design, our point-charge wake function models, Eqs. (4) and (10), should be applicable to any other cavities that utilize smooth nonlinear transitions to the outside beam pipes. These are very common, especially among superconducting "bell-shaped" designs, used both in light sources and collider accelerators. Multicell cavities or multiple single-cell ones placed close together in a single cryostat are also common. As we showed in Sec. III B, our point-charge wakefield models are also applicable to these cases and the savings in computational effort compared to direct wakefield calculations could be very substantial. For instance, one of the presently considered main rf cavity arrangements for the electron storage ring in the Electron-Ion Collider [23] is to place each pair of 591 MHz cavities in a single cryostat. If the two cavities are separated by about 1 m and each directly transitions to a 75 mm radius beam pipe outside, then the λ_g parameter is on the order of 1 cm. This implies that a 1-mm rms long bunch is short enough to reconstruct the point-charge wakefield for such a fairly large structure and to avoid direct pseudo-Green function calculations typically performed at 0.3 mm for this ring.

To conclude, we believe that the proposed model is quite general and applicable to a large number of cavity designs. We also believe that the method of calculating point-charge wakefield for realistic cavities by fitting to this model is rather powerful and could substantially save both computational and personal time and effort.

ACKNOWLEDGMENTS

We thank the third harmonic cavity collaboration among CELLS, HZB, and DESY. We would like to acknowledge Jesús Ocampo and Volker Dürr for the CAD model of the cavity and Markus Ries for the discussion of potential applications of the cavities. We also thank Igor Zagorodnov for his help with the ECHO code. Finally, we thank Andreas Jankowiak, Markus Ries, Aleksandr Matveenko, and Michael Blaskiewicz for the careful reading of the manuscript and their insightful comments. B. P.'s work is supported by Brookhaven Science Associates, LLC under Contract No. DE-SC0012704 with the U.S. Department of Energy.

[1] S. A. Heifets and S. A. Kheifets, Coupling impedance in modern accelerators, Rev. Mod. Phys. **63**, 631 (1991).

[2] A. W. Chao, *Physics of Collective Beam Instabilities in High Energy Accelerators* (John Wiley & Sons, Inc., New York, 1993).

[3] X. Deng, A. Chao, J. Feikes, A. Hoehl, W. Huang, R. Klein, A. Kruschinski, J. Li, A. Matveenko, Y. Petenev, M. Ries, C. Tang, and L. Yan, Experimental demonstration of the mechanism of steady-state microbunching, Nature (London) **590**, 576 (2021).

[4] A. Blednykh, G. Bassi, V. Smaluk, and R. Lindberg, Impedance modeling and its application to the analysis of the collective effects, Phys. Rev. Accel. Beams **24**, 104801 (2021).

[5] D. Wang, K. Bane, D. Li, T. Luo, O. Omolayo, G. Penn, S. De Santis, C. Steier, and M. Venturini, Broadband impedance modeling and single bunch instabilities estimations of the advanced light source upgrade project, Nucl. Instrum. Methods Phys. Res., Sect. A **1031**, 166524 (2022).

[6] W. Anders and P. Kuske, HOM damped NC passive harmonic cavities at BESSY, in *Proceedings of the 2003 Particle Accelerator Conference, Portland, OR* (IEEE, New York, 2003), pp. 1186–1188.

[7] B. Bravo, J. Alvarez, F. Pérez, and A. Salom, 1.5 GHz Cavity Design for the CLIC Damping Ring and as Active Third Harmonic Cavity for ALBA, in *Proceedings of the 8th International Particle Accelerator Conference, Copenhagen, Denmark* (JACoW, Geneva, Switzerland, 2017), pp. 4263–4265.

[8] F. Pérez, W. Anders, V. Dürr, M. Ebert, P. Hülsmann, T. Loewner, A. Matveenko, W. Müller, J. Ocampo, R. Onken, M. Ries, A. Salom, L. Shi, P. Solans, Y. Tamashevich, and A. Tsakanian, 3HC—third harmonic normal conducting active cavity collaboration between HZB, DESY and ALBA, in *Proceedings of 13th International Particle Accelerator Conference, IPAC-2022, Bangkok, Thailand* (JACoW, Geneva, Switzerland, 2022), pp. 1471–1474.

[9] Goslawski *et al.*, BESSY III & MLS II—Status of the development of the New Photon Science Facility in Berlin, in *Proceedings of 12th International Particle Accelerator Conference, IPAC-2021, Campinas, SP, Brazil* (JACoW, Geneva, Switzerland, 2021), pp. 451–454.

[10] J. Feikes, M. Von Hartrott, M. Ries, P. Schmid, G. Wüstefeld, A. Hoehl, R. Klein, R. Müller, and G. Ulm, Metrology light source: The first electron storage ring optimized for generating coherent THz radiation, Phys. Rev. ST Accel. Beams **14**, 030705 (2011).

[11] B. Podobedov and G. Stupakov, Point-charge wakefield calculations from finite length bunch wake potentials, Phys. Rev. ST Accel. Beams **16**, 024401 (2013).

[12] B. Podobedov and G. V. Stupakov, New method for point-charge wakefield calculation, in *Proceedings of North American Particle Accelerator Conference, Pasadena, CA, 2013* (JACoW, Geneva, Switzerland, 2013), pp. 778–780.

[13] I. Zagorodnov, Echo code, https://echo4d.de/ (2022).

[14] K. Y. Ng and K. Bane, Explicit expressions of impedances and wake functions, in *Handbook of Accelerator Physics and Engineering*, 2nd ed., edited by A. W. Chao, K. H. Mess, M. Tigner, andF. Zimmermann (World Scientific, Singapore, 2013), Chap. 3, Sec. 3.2.4.

[15] K. L. F. Bane and M. Sands, Wakefields of very short bunches in an accelerating cavity, Part. Accel. **25**, 73 (1987).

[16] B. Podobedov, Short-range wakefields of slowly tapered structures, in *Proceedings of IPAC2012, New Orleans, Louisiana, USA* (IEEE, Piscataway, NJ, 2012)), WEPPR100.

[17] G. Stupakov, K. L. F. Bane, and I. Zagorodnov, Impedance scaling for small angle transitions, Phys. Rev. ST Accel. Beams **14**, 014402 (2011).

[18] W. K. H. Panofsky and W. Wenzel, Some considerations concerning the transverse deflection of charged particles in radiofrequency fields, Rev. Sci. Instrum. **27**, 967 (1956).

[19] Y. H. Chin, ABCI code, https://abci.kek.jp/abci.htm (2022).

[20] SLAC, Ace3p, https://conf.slac.stanford.edu/cw18/sites/cw18.conf.slac.stanford.edu/files/broc-ace3p.pdf (2022).

[21] CST particle studiohttps://www.3ds.com/products-services/simulia/products/cst-studio-suite/ (2022).

[22] W. Bruns, Gidfidl code, http://www.gdfidl.de/ (2022).

[23] F. Willeke and J. Beebe-Wang, Electron ion collider conceptual design report 2021, Brookhaven National Laboratory (BNL), Upton, NY, Technical Report No. BNL-221006-2021-FORE, 2021.